

Article

Development of a Binder-Free Tetra-Metallic Oxide Electrocatalyst for Efficient Oxygen Evolution Reaction

Muhammad Asad ¹, Afzal Shah ^{1,*} , Faiza Jan Iftikhar ², Rafia Nimal ¹, Jan Nisar ³  and Muhammad Abid Zia ⁴

¹ Department of Chemistry, Quaid-i-Azam University, Islamabad 45320, Pakistan; muhammadasad284@yahoo.com (M.A.); rafia.numal@gmail.com (R.N.)

² NUTECH School of Applied Sciences and Humanities, National University of Technology, Islamabad 44000, Pakistan; faizajiftikhar@nutech.edu.pk

³ National Centre of Excellence in Physical Chemistry, University of Peshawar, Peshawar 25120, Pakistan; pashkalawati@gmail.com

⁴ Department of Chemistry, University of Education Lahore, Attock Campus, Attock 43600, Pakistan; abid@ue.edu.pk

* Correspondence: afzals_qau@yahoo.com

Abstract: Water splitting has emerged as a sustainable, renewable and zero-carbon-based energy source. Water undergoes hydrogen evolution reaction (HER) and oxygen evolution reaction (OER) during electrolysis. However, among these half-cell reactions, OER is more energy demanding. Hence, the development of efficient catalysts for speeding up OER is a key for boosting up the commercial viability of electrolyzers. Typical binders like Nafion and PVDF are not preferred for designing commercial electrocatalysts as they can compromise conductivity. Thus, we have designed a novel and cost-effective binder-free tetra-metallic (Co-Cu-Zn-Fe) oxide catalyst that efficiently catalyzes OER. This catalyst was grown over the surface of Fluorine doped tin oxide (FTO) transducer by a facile potentiodynamic method. The structure and morphology of the modified electrode were characterized by X-ray diffraction (XRD), scanning electron microscopy, and energy dispersive X-ray spectroscopy. XRD analysis confirmed the deposition of CoFe_2O_4 and CuCo_2O_4 along with alloy formation of Co-Fe and Co-Cu. Similarly, EDX and SEM results show the presence of metals at the surface of FTO in accordance with the results of XRD. Linear scan voltammetry was employed for testing the performance of the catalyst towards accelerating OER in strongly alkaline medium of pH-13. The catalyst demonstrated stunning OER catalytic performance, with an overpotential of just 216 mV at 10 mA cm^{-2} current density. Moreover, the chronopotentiometric response revealed that the designed catalyst was stable at a potential of 1.80 V for 16 h. Thus, the designed catalyst is the first example of a highly stable, efficient, and inexpensive catalyst that catalyzes OER at the lowest overpotential.

Keywords: electrocatalyst; water splitting; oxygen evolution reaction; low overpotential; tetra-metallic oxide-based catalysts



Citation: Asad, M.; Shah, A.; Iftikhar, F.J.; Nimal, R.; Nisar, J.; Zia, M.A. Development of a Binder-Free Tetra-Metallic Oxide Electrocatalyst for Efficient Oxygen Evolution Reaction. *Sustain. Chem.* **2022**, *3*, 286–299. <https://doi.org/10.3390/suschem3030018>

Academic Editor: Roger Gläser

Received: 6 May 2022

Accepted: 31 May 2022

Published: 21 June 2022

Publisher's Note: MDPI stays neutral with regard to jurisdictional claims in published maps and institutional affiliations.



Copyright: © 2022 by the authors. Licensee MDPI, Basel, Switzerland. This article is an open access article distributed under the terms and conditions of the Creative Commons Attribution (CC BY) license (<https://creativecommons.org/licenses/by/4.0/>).

1. Introduction

The industrial revolution and population growth have led to an increase in energy demands. Though fossil fuels have been satisfying most energy requirements, their combustion generates carbon dioxide, which is a major source of global warming. Moreover, reserves of fossil fuels are being depleted. These alarming implications have compelled the scientific community to explore renewable and sustainable energy resources to comply with increasing energy demand and environmental friendliness. Among the plethora of clean energy resources that have been probed so far, energy generation from water is attracting increased attention, as water is found in abundance. Hence, concerted efforts are underway to develop efficient catalysts for energy generation from water [1].

Solid-state catalysts employing noble metals, such as platinum, gold, and non-noble titanium metal, have long been documented as being proficient HER catalysts, while ruthenium and iridium-based metals catalyze OER at lower overpotentials. Nevertheless, their exorbitant prices and scarce availability limit their applications. These catalysts have additionally been found to be susceptible to poisoning due to harsh reaction conditions [2], which results in their activity being impeded, limiting the large scale commercialization of electrolyzers using these catalysts. Therefore, it is highly desirable to search for cost-effective water splitting catalysts. The last few years have witnessed a mushrooming of several favorable solid-state HER/OER catalysts made up of transition and earth-abundant metals. For example, molybdenum sulfides $M\text{-Mo}_2\text{S}$ ($M = \text{Fe, Co, Ni, etc.}$) of varying morphologies have been identified and reported to be active HER/OER catalysts [3–7]. Similarly, MoB , Mo_2C , and Cu_2MoS have also been documented to show promising HER/OER catalysis [4–7]. First-row transition elements such as $\text{H}_2\text{-CoCat MS}_2$, ($M = \text{Fe, Co, Ni, etc.}$), CoP , CoSe_2 , Co-NRCNT , FeS , FeP , and Ni_2P have been extensively studied for their enhanced catalytic activities [8]. However, these catalysts are frequently pre-treated in strongly acidic electrolytes, while some of them demand treatment with toxic gases at elevated temperatures.

Researchers have been trying to explore OER catalytic performance by employing individual earth abundant metals as well as seeking their synergistic combinations as viable catalysts for electrolyzers. In this regard, some hybrid catalysts, for instance Cu nanoparticles incorporated into CoS_x , have displayed good activity and stability for OER [9]. Cu prevents the corrosion issue of Co oxides [1]. Likewise, copper and Zn are used in electrolyzers to minimize or avoid corrosion problems and to consequently catalyze water splitting reactions efficiently. Iron-based catalysts have also been found to accelerate OER in electrolyzers [10]. However, corrosion is still an issue when it is attempted to use iron alone for OER. To enhance the corrosion resistivity of iron, it must be alloyed with other metals such as Co, Ni, Mo, Cu, Zn [9]. In this regard, Renato et. al. found that Ni-Fe-Mo ternary catalyst exhibits efficient catalytic activity towards HER/OER [11]. Similarly, Jafarian et. al. reported that nanocrystalline Co-Ni-Fe shows improved catalytic activity compared to individual metals or their binary combinations [1]. Akbar et al. attempted to synergistically combine CuZnAg non-noble metals for efficient OER activity [12]. Furthermore, it has been established that OER stability can be enhanced by a CuO electrocatalyst. It has been demonstrated that CuO enhances the stability of the catalyst due to its nanoblock morphology and it has been shown to exhibit an overpotential (η) of 475 mV in a 1.0 M KOH at 10 mA cm^{-2} [13]. Likewise, ZnO- CoO_x nanospheres have been prepared by the method of co-electrodeposition of Co-Zn alloy, which is then electrochemically corroded. Zn has been shown to play an important role in the nanostructured morphology, enhancing the active surface area and hence resulting in enhanced activity and stability for OER [14]. Similarly, CuCoO nanowires showed high stability and electrocatalytic activity for OER in a 1.0 M KOH solution than the benchmark IrO_2 [15,16]. These nanowires are grown on Ni foam and have been shown to contain crystals of Cu_2O , CoO and CuCo_2O_4 with variable oxidation states. Fe and O is doped in Co_2P to form CoFePO , which consists of nanoparticles arranged as nanowires and employed to enhance the stability and activity of the catalyst [17]. Furthermore, efforts have been directed towards using binder-free modified electrodes to improve the conductivity of the working matrix. A binder is usually used to bind the catalyst to the surface of the electrode. Some commonly used binders are Triton X-100, Nafion, sodium dodecyl sulfate, cetyltrimethylammonium bromide, etc. However, binders have been observed to inhibit the catalytic activity by blocking the active sites and as a result low current value and a high onset potential are obtained which are contrary to what is desired for an efficient electrocatalyst. Therefore, researchers are trying to develop binder-free electrocatalysts for OER activity [12,18–20].

The search for more effective electrocatalysts utilizing synergistic properties by combining metals imparting distinctive properties to a composite has attracted considerable attention. However, it is a rather challenging task to combine metals in proportions and

combinations that may lead to favorable enhancement of synergistic properties. Herein, we report a Co, Cu, Zn and Fe oxide-based tetra-metallic electrocatalyst on Fluorine-doped tin oxide (FTO) as a support that catalyzes OER with an exceptional overpotential. FTO has been found to be relatively stable at high cathodic and anodic potentials, which was the reason for this choice [21]. This cheaper corrosion- and binder-free metal oxide-based catalyst with good conducting properties synthesized by a simple in situ one pot electrochemical method, is the most promising addition to the list of low-cost catalysts for accelerating OER at a lower overpotential. This is accomplished by employing abundantly available transition metals. From a practical point of view, this is the first reported work on a tetra-metallic catalyst with a significantly low overpotential and holds great promise for use as a proof of concept for the commercial application of alkaline electrolyzers.

2. Experimental

2.1. Chemicals and Instrumentation

Analytical-grade chemicals (listed in Table 1) were used during the synthesis of the electrocatalyst. All solutions were prepared in deionized water with resistivity of 18 mΩ.

Table 1. List of deposited materials.

Alloy Name	Chemical Formula	Peak Position (2θ)	Crystal Type	Space Groups	hkl
Cuprospinel	CuFe ₂ O ₄	29.81	Tetragonal	F	202
		35.93			311
Zinc Iron Oxide	ZnFe ₂ O ₄	37.11	Cubic	Fd3m	222
		43.03			400
Copper Zinc Oxide	CuZnO ₂	49.77	Cubic	Pm3m	200
Cobalt Iron Oxide	CoFe ₂ O ₄	57.15	Cubic	Fd3m	511
		65.17			440
Copper Cobalt Oxide	CuCo ₂ O ₄	77.57	Cubic	Fd3m	533

Electrochemical experiments were performed by means of computer-controlled potentiostat Metrohm Autolab PGSTAT-M101A running with NOVA 1.11 software. Cyclic voltammetry (CV), chronoamperometry (CA) and linear sweep voltammetry (LSV) were performed in a three-electrode system. Ag/AgCl (3 M KCl) and platinum wire were used as reference and counter electrodes, respectively. FTO was used as a working electrode. It was washed with acetone under sonication for 15 min. The same process was then repeated with deionized water prior to electrode modification. Cyclic voltammetry was performed to characterize the reduction potential of respective metal ions which were then electrodeposited over FTO surface via controlled potential electrolysis (CPE). X-ray diffraction (XRD) patterns were recorded directly on the modified electrode using Bruker Focus D8 via ceramic mono chromatized Cu Kα radiation of 1.54178 Å with a scanning range of 5–70° operated at 5° per min in 2θ at 45 kV and 45 mA. Scanning electron microscopy (SEM) micrographs and energy dispersive X-ray (EDX) spectra were obtained on Hitachi S-4800 (Hitachi, Japan) equipped with a Horiba EDX system (X-max, silicon drift X-ray detector). SEM images were taken with an acceleration voltage of 5 kV, while EDX mapping images and spectra were recorded with acceleration voltages of 20 kV with a scanning time of 20 min.

2.2. Method of Electrode Modification

In situ electrochemical methods were employed for the electrodeposition of metals over the FTO surface. Stock solutions of 1 M copper sulfate, iron sulfate, cobalt sulfate and zinc sulfate were prepared. Each solution was prepared by dissolving the respective amounts of salts in 100 mL of deionized water. Working solutions were prepared

by diluting the stock solutions to the desired concentration. Cyclic voltammetry was employed to investigate the reduction potential of the respective metals in alkaline medium of pH 13.0 using 1 M KOH as a supporting electrolyte. After confirmation of reduction potentials, chronoamperometry (potentiostatic) was carried out for in situ electrodeposition of metal ions at the chosen reduction potential on FTO surface according to the method reported in literature [9]. Moreover, equal volumes of all the four metal sulfate ($\text{CoSO}_4 + \text{CuSO}_4 + \text{ZnSO}_4 + \text{FeSO}_4$) solutions were taken in 100 mL beaker by taking 25 mL of them each. Further, 25 mL of the mixed metallic sulfate solution was taken in an electrolytic cell and added to a 25 mL of supporting electrolyte (1 M KOH) of pH 13. For electrodeposition of tetra-metallic ions, controlled potential electrolysis (CPE) at three different values of deposition potentials (-1.3 V, -1.4 V and -1.5 V) was performed for 15 min. The molar ratio of the combined metals was optimized. The best combination was used for the investigation of the oxygen evolution reaction. After electrodeposition of metal ions on the FTO surface, linear sweep voltammetry (LSV) was employed to investigate the OER activity of individual metals as well as the tetra-metallic electrocatalyst. Prior to recording LSV, the electrode was conditioned by cycling the potential between 0 to 1.5 V for several cycles for achievement of reproducible voltammograms. All potentials unless otherwise stated were calibrated against Reference Hydrogen Electrode (RHE) for the electrolyte used to investigate water splitting.

3. Results and Discussion

3.1. Cyclic Voltammetry

CV was employed to acquire redox signals of the respective metallic ions in basic medium at the bare FTO electrode. CVs of individual metal ions in 1 M KOH are shown in Figure S1. For Co^{2+} , a decrease in current at -0.6 V followed by a sharp peak at -1.3 V is observed (Figure S1a), corresponding to the reduction of the Co^{2+} ions at the electrode surface with a current cross-over at -1.4 V in the reverse cycle. This current cross-over can be related to the nucleation growth process at FTO surface [22]. A sharp oxidation signal around -1.0 V corresponds to the stripping of Co^{2+} ions off the FTO surface back into the solution [23]. Similarly, for Cu^{2+} in Figure S1b reduction occurs at -0.2 V while oxidation peak corresponding to stripping off the electrodeposited copper back into the solution, appears at 0.6 V [9]. In case of Fe^{2+} (Figure S1c) the reduction peak appears at -1.17 V with corresponding oxidation signal at -0.38 V. These values match well with literature reported redox potentials of Fe^{2+} [9]. Likewise, CV of zinc reveals (Figure S1d) a slight decrease in current at -0.6 V in the reduction scan, which continues further to a sharp decrease in current at -1.3 V corresponding to the reduction of Zn^{2+} at the FTO surface. A current crossover at -1.19 V corresponds to the onset of nucleation growth of zinc at the FTO surface while oxidation peak at -0.6 V relates to the stripping of zinc ions at the FTO surface as a result of the oxidation process [1]. The difference between the highest value of current generated by the FTO in both the forward and reverse scans decides whether the process of reduction of analyte or its oxidation is faster. From the CV results, reduction potential, oxidation potential, highest reductive current, and highest oxidative current of the individual metal ions were determined. The effect of 50 successive CV scan cycles on the redox peaks of cobalt, copper, zinc, and iron was additionally investigated. With increasing number of scan cycles, the intensity of reduction signals increased up to 50th cycle (Figure S2), leading to the growth of metals over the electrode surface as reported previously [1]. The catalyst modified electrode was then subjected to water splitting performance. The details are given vide infra.

3.2. Electrodeposition through Chronoamperometry

Chronoamperometry was applied for in situ deposition of individual metal ions on FTO surface in an aqueous medium of 1 M KOH as shown in Figure S3 at various deposition potentials via CPE with a deposition time of 15 min. Observation of Figure 1 reveals that at the commencement of the applied potential, cathodic current intensifies quickly which after

a short time rapidly decreases due to possible depletion of metal ions from the electrode surface. Finally, a steady value of current is approached. In all cases, it was noticed that with increasing deposition potential, the value of generated current increased, thereby suggesting a high amount of metal ions being deposited on the FTO surface at -1.5 V.

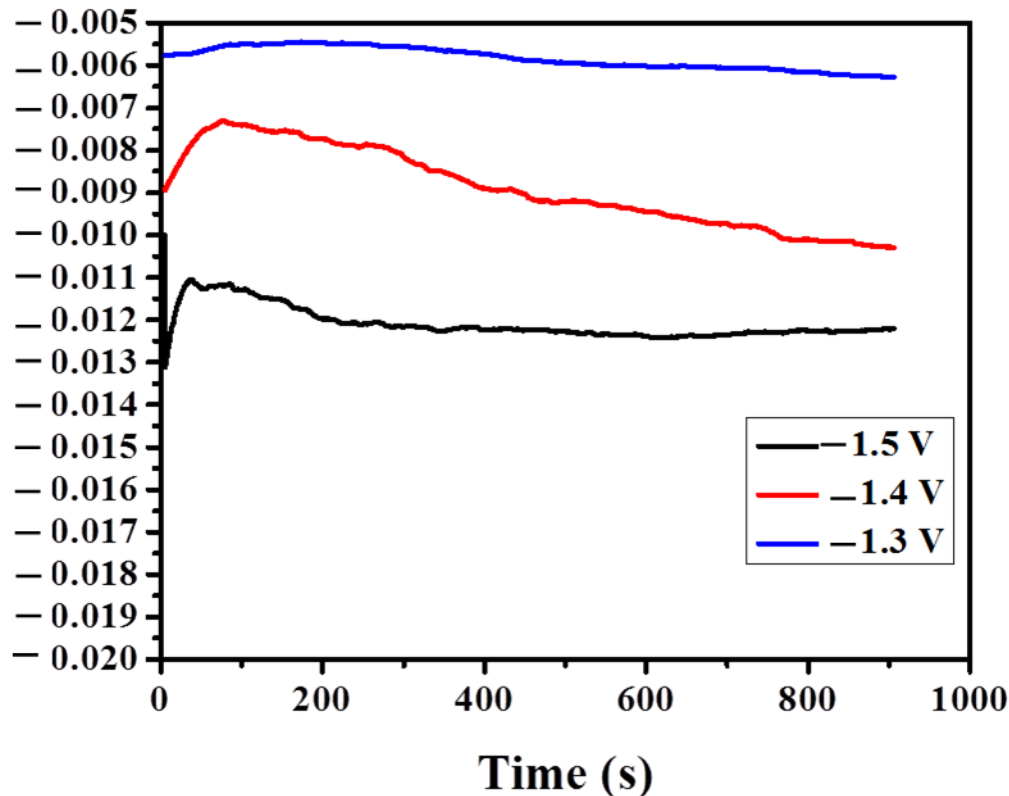


Figure 1. In situ deposition of Co-Cu-Fe-Zn oxides simultaneously on FTO at different values of deposition potential using 1 M KOH as a supporting electrolyte for 900 s.

In chronoamperometry, the value of current density depends upon overpotential. This is associated with the nucleation growth process of the catalyst. After some time, the current attains a steady value, suggesting that the process is diffusion-controlled, as described by the Cottrell equation (Equation (1)).

$$i = \frac{nFAC^0j\sqrt{Dj}}{\sqrt{\pi t}} \quad (1)$$

Figure 1 demonstrates the simultaneous deposition of the tetra-metallic oxide electro-catalyst on FTO surface. Like the pattern observed in the chronoamperograms of individual ions, cathodic current enhancement occurred for all four metal ions for a short period of time. Afterwards, due to the depletion of the concentrations of metal ions from the electrode surface, the current starts to decrease gradually because of diffusion controlled regime and a constant value of current is finally approached.

3.3. Characterization of Modified FTO

3.3.1. XRD Analysis of FTO Modified with Tetra-Metallic Electro-Catalyst

The XRD spectra recorded directly on the FTO with metal films coated at -1.50 V vs. Ag/AgCl (3 M KCl) are presented in Figure 2. The XRD spectra confirms the presence of oxides of Co, Cu, Fe, and Zn on FTO apart from the signals originating from bare FTO.

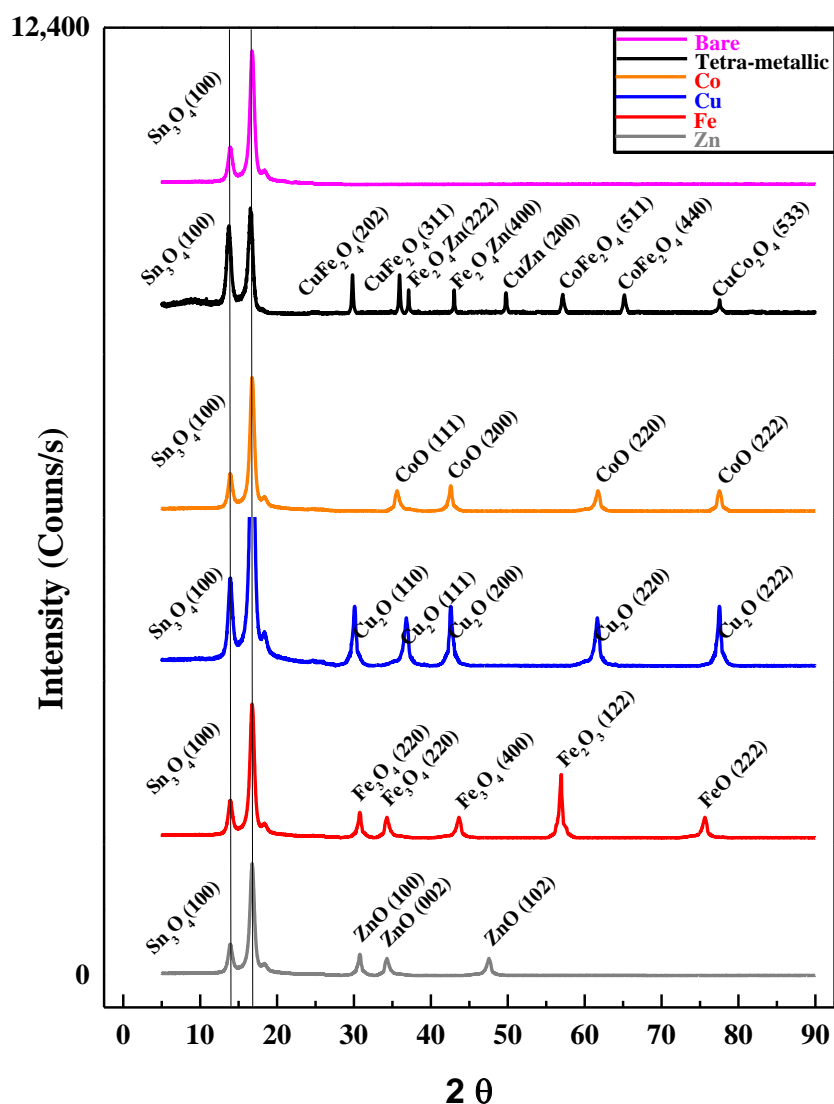


Figure 2. XRD patterns of the FTO with deposited films of oxides of tetra-metallic (Co-Cu-Fe-Zn) Catalyst in 1 M KOH (pH = 13) at deposition potentials of -1.5 V.

For bare FTO (Figure 2), two strong peaks are observed at 13.93° and 16.75° . The peak at 16.75° corresponds to cubic FTO with hkl values of (111) [24] and the peak at 13.93° corresponds to monoclinic fluorine tin oxide with hkl values of (-110) [25]. Meanwhile, for tetra-metallics, the first two peaks in the region of 10° to 20° represent characteristic peaks of FTO. The peaks at 35.91° , 42.59° , 61.73° , and 77.53° correspond to cubic cobalt oxide (CoO) with hkl facets of (111), (200), (220), and (222), respectively [26]. These peak positions were previously reported by Masoumeh et al.; however, in the case of our modified electrode, an additional peak is observed at 77.549° [27]. The peak pattern observed in our case matches with the reference code number JCPDS-00-001-1227. Similarly, the XRD pattern for Cu (blue spectra) represents the deposition of copper over FTO. Other than the two FTO peaks between 10° to 20° , there are five additional peaks at 2θ values of 30.09° , 36.81° , 42.59° , 61.65° , and 77.53° corresponding to cubic copper oxide (Cu_2O) with hkl facets of (110), (111), (200), (220), and (222), respectively [26]. This peak pattern has previously been reported by Esmaeeli et al., with an additional peak at 77.53° [28]. The peak matches with the reference code number of JCPDS-00-001-1142. The XRD pattern of Fe confirmed the deposition of iron over FTO. After the region of 10° to 20° (FTO region), there are five peaks at 30.69° , 34.29° , 43.65° , 56.95° , and 75.63° . The first three peaks correspond to cubic magnetite (Fe_3O_4) with hkl facets of (221), (220) and (400), respectively. Peak match

was confirmed with reference code number JCPDS-01-074-1910 [22]. The peak located at 56.95° corresponds to rhombohedral Hematite (Fe_2O_3) with hkl facet of (122), which was confirmed and matched with reference code number JCPDS-00-001-1053 [26]. Similarly, the peak position of 75.63° corresponds to cubic iron oxide (FeO) with hkl facets of (222), which matched with reference code number JCPDS-00-001-1223 [26]. Fondell et al. studied the phase control iron oxide over FTO, and reported the formation of Magnetite, Hematite and FeO in a similar region [29]. The grey-colored peak represents the deposition of zinc over FTO. After the region of 10° to 20° (FTO region), there are three peaks at 30.77° , 34.29° and 47.55° corresponding to hexagonal zinc oxide (ZnO) with hkl facets of (100), (002), and (102), respectively. The peaks were matched and confirmed with reference code JCPDS-00-001-1136 [26]. Anandhi et al. previously reported similar peaks of ZnO in their study [9].

In Figure 2, the individual peak positions of ZnO (100), Fe_3O_4 (220) and Cu_2O (110) lie in a similar region, $\sim 30^\circ$; thus, alloy formation of the oxides of metals (Cu-Zn), (Fe-Zn), (Cu-Fe) and (Cu-Zn-Fe) is inferred when all of these metals are simultaneously electrodeposited over FTO. Similarly, the peak positions of CoO (111) and Fe_3O_4 (220) occur in a similar range of 2θ ($34.50\text{--}35.50^\circ$), and CoO (200) while Fe_3O_4 (400) also occur in a close range of ($42.50\text{--}43.50^\circ$); thus, alloy formation of the oxides of (Co-Fe) is also expected, and the individual peak positions of Cu_2O (200)/CoO (200), Cu_2O (220)/CoO (220) and Cu_2O (222)/CoO (222) coincide at 43° , 62° and 77° ; thus, an alloy of the oxides of (Co-Cu) can also be expected during simultaneous electrodeposition of these metals. Peaks at 29.81° and 35.93° correspond to Tetragonal Copper Iron Oxide (Cuprospinel CuFe_2O_4) with hkl facets of (202) and (311), respectively. Peaks were confirmed and matched with reference code number JCPDS-00-025-0283 [30]. Similarly, the peak positions at 37.11° and 43.03° correspond to Cubic Zinc Iron Oxide (ZnFe_2O_4) with hkl facets of (222) and (400), respectively. Respective peaks were confirmed and matched with reference code number JCPDS-00-001-1108 [31]. A peak appearing at 49.77° corresponding to Cubic Copper Zinc (Brass CuZn) with single hkl facet of (200) was confirmed and matched with reference code number JCPDS-00-006-0657 [32]. Peaks occurring at 57.15° and 65.17° correspond to Cubic Cobalt Iron Oxide (CoFe_2O_4) with hkl facets of (511) and (440), respectively. Peaks were matched and confirmed with reference code number JCPDS-00-001-1121 [33]. The last peak in our analysis occurred at 77.57° , corresponding to a single hkl facet (533) of Cubic Copper Cobalt Oxide (CuCo_2O_4). The peak was matched and confirmed with reference code number JCPDS-00-001-1155.

Table 1 depicts the metal oxide alloys that were observed in the electrodeposited tetra-metallic electrocatalyst over FTO. Out of eight metal oxide alloys, six contained iron as the main constituent, while the remaining two alloys, i.e., brass and cobalt copper oxide, contained copper as the main constituent. Thus, one can expect the formation of multiple metal oxide alloys when varying the concentration of the source metallic solutions, which will be further probed in future studies. Another factor that governs the quality of metal oxide alloy formation is the respective deposition time. Lastly, the applied potential also plays an important role in determining the quality of the deposited material [1,11,34–42].

3.3.2. SEM and EDX Analysis of FTO Modified with Oxides of Tetra-Metallic Electrocatalyst

SEM analysis is performed to examine and analyze the morphology of diverse materials. This specific technique provides us with crucial information about surface roughness, porosity, inter-metallic distribution, material homogeneity, and particle size. The SEM analysis (Figure 3) offers evidence about film formation of the synthesized catalyst over the surface of FTO. In SEM micrographs, regular cubic shape particles can be observed spread out randomly throughout the surface. This suggests uniform deposition of metal oxides with different shapes. Additionally, under magnification to $5\ \mu\text{m}$ in Figure 3e, the growth is confirmed to be of tetrahedral-type particles.

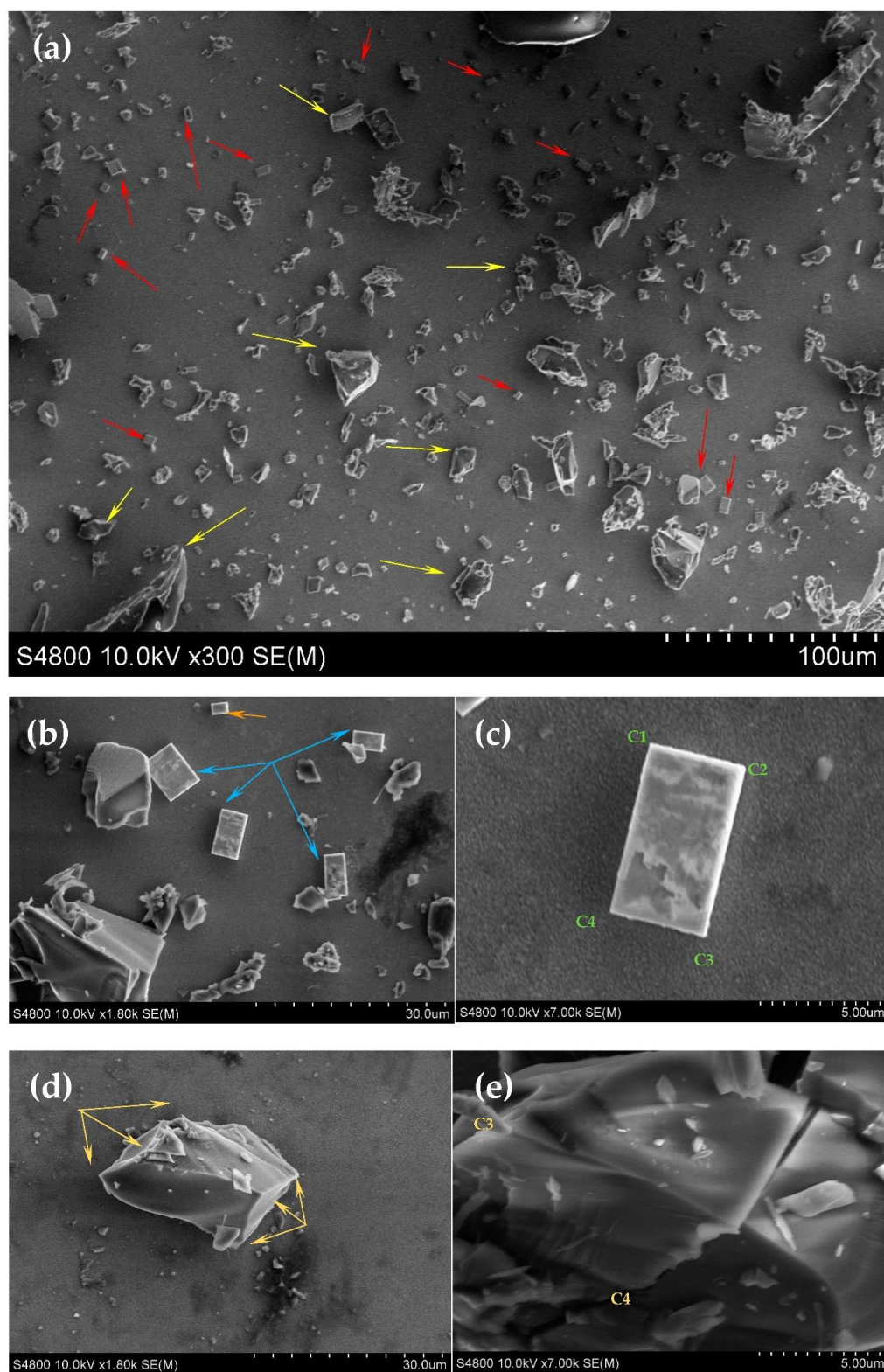


Figure 3. SEM images of Co-Cu-Fe-Zn oxide films obtained by electrodeposition in basic medium (pH-13) at -1.5 V. (a) SEM micrograph taken at $100\ \mu\text{m}$, arrows showing random distribution of cubic and tetragonal particles; (b) SEM micrograph of cubic particles magnified at $30\ \mu\text{m}$; (c) SEM micrograph of cubic particles magnified at $5\ \mu\text{m}$; (d) SEM micrograph of tetragonal-shaped particles magnified at $30\ \mu\text{m}$ as indicated by arrows; (e) SEM micrograph of tetragonal-shaped particles magnified at $5\ \mu\text{m}$.

EDX was performed to detect the presence of metals on the FTO surface. Figure 4 shows an EDX image of the designed electrocatalyst film coated over FTO surface at -1.5 V deposition potential. The presence of all four metals is evident, and this result is in accordance with the XRD analysis. Based on the EDX results the percentage of individual metals in the deposited film is tabulated in Table 2. The Sn and O appearing in the above analysis comes from FTO, while the metals are components of the film deposited under de-aerated conditions. It can be seen that the relative atomic and weight percentage of iron is almost 2 times that of the remaining three metals, as during deposition, 4 mM of iron was used in the solution, while concentrations of the remaining three metals were 2 mM.

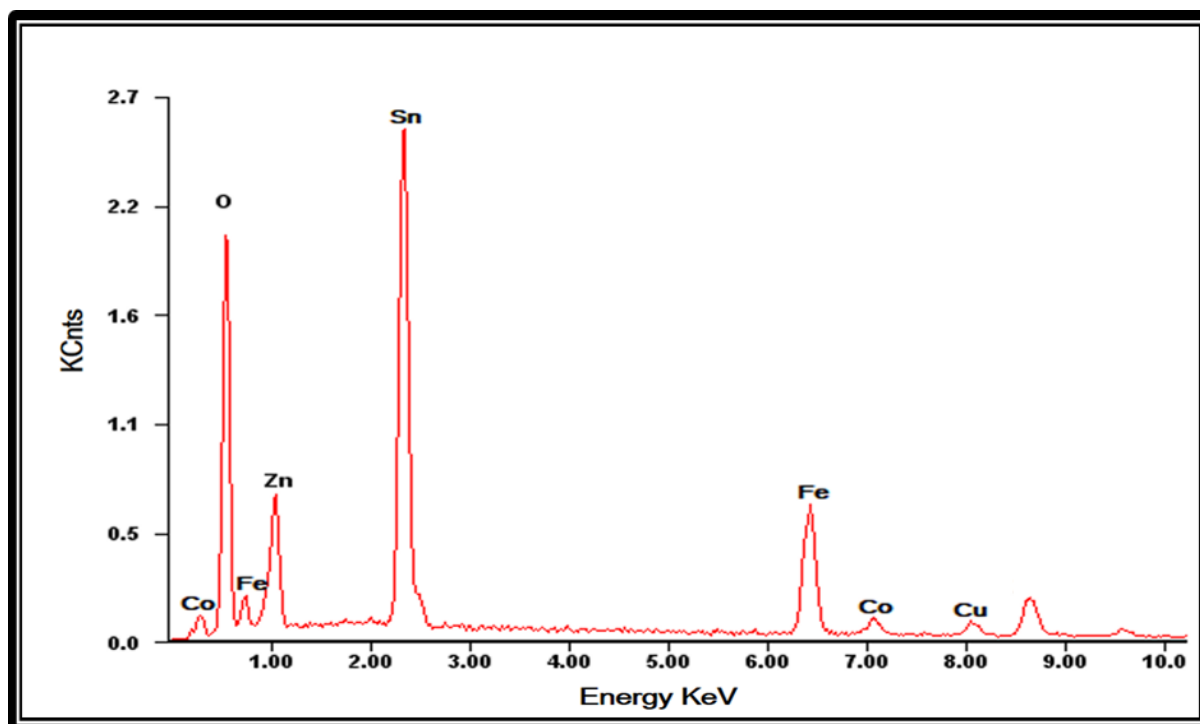


Figure 4. EDX image of Co-Cu-Zn-Fe oxides-based deposited films in basic medium at -1.5 .

Table 2. wt.% and at.% of tetra-metallic thin film coated on FTO.

Element	wt.%	at.%
Sn	41.07	51.12
O	33.72	32.74
Cu	4.50	1.54
Zn	6.04	2.83
Fe	10.61	9.74
Co	4.06	2.03

3.4. Linear Sweep Voltammetry for the OER Activity of the Catalyst

OER activity for the modified FTO was investigated through LSV. Figure 5a demonstrates the LSV curves of the electrosynthesized catalyst grown over the FTO surface in 1 M KOH at a scan rate of 10 mV/s. The potentials were measured with respect to Ag/AgCl (3 M KCl) and converted to the RHE scale according to the equation: $E_{RHE} = E_{Ag/AgCl} + 0.0591 \text{ pH} + E^{\circ}_{Ag/AgCl}$. The overpotential was evaluated from the relation $\eta = V_{app} - iR - E_{pH}$, where i denotes the stable current, R the uncompensated resistance (measured with the help of impedance spectroscopy for both modified and bare FTO), V_{app} the applied potential vs. RHE, and E_{pH} the thermodynamic potential for water oxidation at the pH of the solution of interest ($E_{pH} = 1.230 \text{ V} - 0.059 \text{ pH V vs. RHE}$). It can be seen that in KOH, a current density

of 1 mA/cm^2 is obtained at an onset potential of 1.277 V (vs. *RHE*), where bubbles of oxygen are formed at the FTO surface due to electrocatalytic oxidation of water by the FTO supported tetra-metallic catalyst. The low value of overpotential of 216 mV correlates with the outstanding activity of the catalyst.

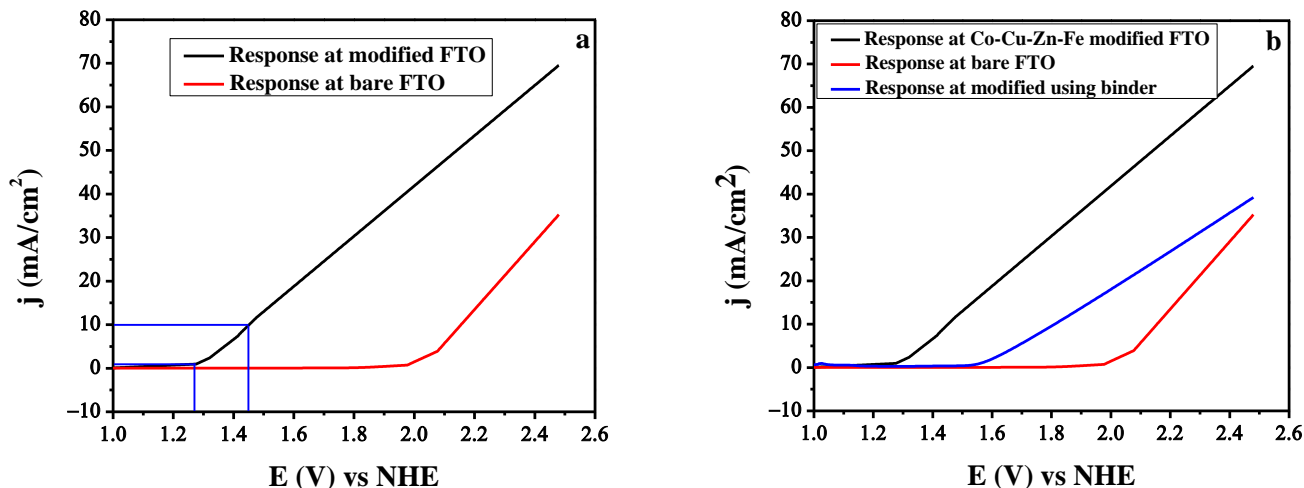


Figure 5. (a) LSV response of Co-Cu-Fe-Zn catalyst in 1 M KOH ($\text{pH} = 13$) at a scan rate of 10 mV/s . (b) LSVs showing the effect of binder on the catalytic performance of modified FTO in KOH ($\text{pH} = 13$) at a scan rate of 10 mV/s .

The LSV curves shown in Figure 5b illustrate the effect of sodium dodecyl sulphate (SDS) binder on the OER performance of Co-Cu-Fe-Zn oxide catalyst anchored over FTO surface. The binder was found to retard the activity of catalyst, as shown by the blue-colored LSV curve, where lower current is recorded compared to binder-free catalyst (black LSV curve). Similar behavior was observed for other binders such as cetyltrimethylammonium bromide, Trion X-100 and Tween 80. Thus, the designed catalyst performs well in the absence of binder.

To explore the stability of the catalyst, CPE was performed in 1 M KOH as shown in Figure 6. The chronoamperogram shows that the catalyst is stable for 16 h . Therefore, based on this behavior, it can be concluded that our catalyst film can effectively catalyze the OER reaction for 16 h in a constant current density range at a potential of 1.80 V .

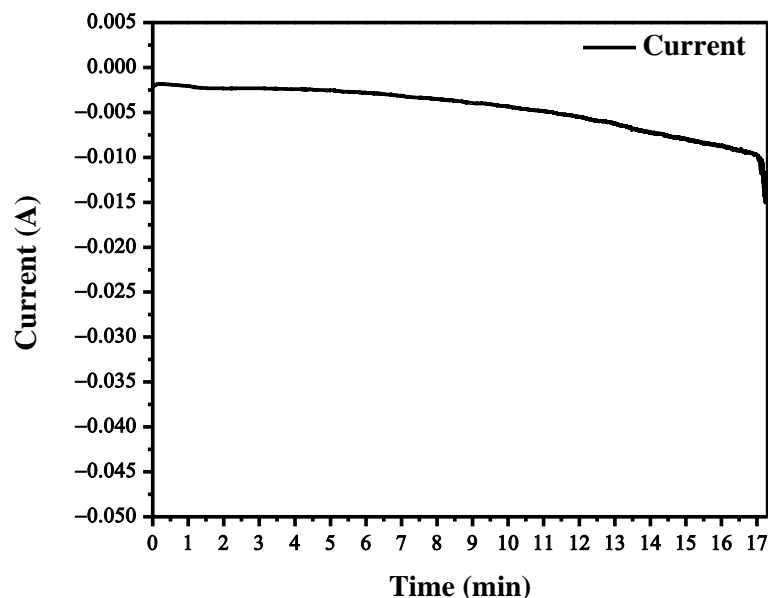


Figure 6. CPE for FTO modified with tetra-metallic electrocatalyst coated for 16 h .

For comparison of the electrocatalytic activity and to clarify the mechanism of reaction of the synthesized electrocatalyst, Tafel analysis was carried out. In general, Tafel slopes are used to extract information about mechanism of electrode reactions, activation energy, role of inhibitors and coatings. Based on these considerations the Tafel plot shown in Figure S4 was obtained. The Tafel slope of 132 mV dec^{-1} obtained by plotting stable current density against overpotential suggests favorable kinetics for OER while reflecting a higher charge transfer ability for the tetra-metallic catalyst. A lower Tafel slope signifies an efficient electrocatalytic performance supported by lower overpotentials. Additionally, it provides insight into the mechanistic pathway of the electrocatalysis. Thus, as in [43], if the first step in the electrode process is a rate determining step, it shows a Tafel slope of 120 mV dec^{-1} . While it is noteworthy that the reaction sequence in any electrode process may display different Tafel slopes depending on which step is the rate determining one as given in [43]. The Tafel slope depends on the transfer coefficient apart from the applied potential and here transfer coefficient is taken as 0.5 for a single electron reaction. While interpreting Tafel slopes, oversimplification of surface coverage is assumed, which may lead to misleading results; hence, for non-ideal real behavior, the experimental observations need to tally with theoretical explanations [12].

The OER performance of the catalyst was assessed with respect to its ability to bring the overpotential closer to 1.230 V (vs. RHE). In the case of Co-Cu-Zn-Fe oxide-modified FTO, OER occurred with a current density of 10 mA/cm^2 at a cell voltage of 1.446 V, which is just 216 mV higher than the theoretical OER potential value of 1.230 V. The current status quo for splitting of water via catalyst is focused on developing transition metal-based catalysts that could catalyze water splitting reactions at lower overpotentials and higher current density. An examination of the data listed in Table 3 reveals that the value of overpotential of our electrosynthesized hybrid catalyst at a current density of 10 mA/cm^2 is much better than the reported ones [14,44–51]. Thus, the designed novel catalyst is the most suitable choice for water splitting owing to its figures of merit with respect to cost affordability, abundant availability, and catalysis of OER at the lowest ever reported overpotential. Thus, our stable and efficient catalyst is a promising candidate for renewable fuel production.

Table 3. Comparison of different metal-based heterogeneous catalysts for oxidation of water in KOH.

Catalyst	η (mV) at 10 mA/cm^2	Refs.
$\text{Fe}_{0.5}\text{Co}_{0.5}\text{O}_x$	257	[44]
$\text{Mn}_3\text{O}_4@\text{Co}_x\text{Mn}_{3-x}\text{O}_4$ Core shell NPs	246	[45]
ZnCo LDH/reduced GO	430	[46]
$\text{CoFe}_2\text{O}_4/\text{C}$	240	
Ternary NiFeMn LDH	310	[47]
$\text{Ni}_2\text{Fe}_1\text{-O}$ NW	244	[48]
$\text{Co}_3\text{Fe}_7\text{O}_x/\text{N-pC-450}$ Nanosphere	328	[49]
ZnO-CoO _x Nanosphere	276	[14]
Iron doped CuS nanocrystal $\text{CuFe}_{0.6}\text{S}_{1.6}$	302	[50]
3D Carbon encapsulated $\text{FeWO}_4\text{-Ni}_3\text{S}_2$ nanosheet	200	[51]
Co-Cu-Fe-Zn oxides	216	This work

The electrochemically active surface area (ECSA = $2250 \text{ cm}^2/\text{g}$) of the FTO modified with tetra-metallic electrocatalyst was calculated by dividing double layer capacitance (C) with specific capacitance ($C_s = 0.040 \text{ mFcm}^{-2}$) using the following equations [52,53]:

$$C = \frac{A}{2vm\Delta V} \quad (2)$$

$$\text{ECSA} = \frac{C}{C_s} \quad (3)$$

where A denotes the integral area of the cyclic voltammogram loop/area under the I–V curve, v the scan rate, m the active mass of electroactive materials and ΔV the potential window in which the voltammogram is recorded. The integral area ($A = 1.08 \times 10^{-4}$ AV) of the cyclic voltammogram obtained at the electrocatalyst-modified FTO was found to be an order of magnitude greater than the A (6.55×10^{-5} AV) obtained at the unmodified FTO.

4. Conclusions

A novel and highly efficient binder-free water-splitting hybrid tetra-metallic electrocatalyst was synthesized by a facile and low-cost electrochemical method using abundantly available transition metals. The deposition of metals on FTO was ensured from the results of XRD, SEM and EDX. The LSV results revealed Co-Cu-Zn-Fe has great potential to contribute to ensuring zero-carbon-based energy economy in future advanced devices for clean energy production by catalyzing OER with considerably higher ECSA, a very low overpotential of only 216 mV at 10 mA/cm², distinctly superior electrocatalytic activity, and stable catalytic performance for 16 h. This extraordinary electrocatalytic activity of Co-Cu-Zn-Fe hybrid tetra-metallic electrocatalyst arises from the synergy among the combined elements of the composite, which requires the selection of the right blend of metals demonstrating synergy.

Supplementary Materials: The following supporting information can be downloaded at: <https://www.mdpi.com/article/10.3390/suschem3030018/s1>. Figure S1: Cyclic voltammogram of individual metal ions in 1 M KOH (a) 2 mM CoSO₄ (b) 2 mM CuSO₄ (c) 4 mM FeSO₄ (d) 2 mM ZnSO₄; Figure S2: Effect of scan cycles on the oxidation/reduction peaks of Co, Cu, Fe & Zn in 1 M KOH at a scan rate of 100 mVs⁻¹; Figure S3: In-situ deposition of (a) cobalt, (b) copper, (c) iron, (d) zinc ions on FTO at different values of deposition potentials in 1 M KOH as supporting electrolyte for a deposition time of 900 s; Figure S4: Tafel plot using data obtained at a scan rate of 10 mV/s in 1 M KOH at the FTO modified with Co-Cu-Zn-Fe.

Author Contributions: Conceptualization, M.A., A.S., F.J.I., R.N.; Data curation, M.A., J.N., M.A.Z.; Formal analysis, M.A., F.J.I., R.N.; Funding acquisition, A.S., J.N., M.A.Z.; Investigation, M.A., A.S., R.N., F.J.I., J.N., M.A.Z.; Methodology, M.A., A.S., R.N., F.J.I., J.N., M.A.Z.; Project administration, A.S., J.N., M.A.Z.; Resources, R.N., F.J.I., J.N., M.A.Z.; Software, M.A., A.S., F.J.I.; Supervision, A.S., J.N., M.A.Z.; Validation, F.J.I., R.N.; Visualization, M.A., A.S., F.J.I.; Writing-original draft, M.A., A.S., F.J.I., R.N.; Writing-review & editing, R.N., J.N., M.A.Z. All authors have read and agreed to the published version of the manuscript.

Funding: The Higher Education Commission of Pakistan is gratefully acknowledged for NRPU Project No. 6815.

Institutional Review Board Statement: Not applicable.

Informed Consent Statement: Not applicable.

Data Availability Statement: The data presented in this study and in the supplementary materials are available on request from the corresponding author.

Acknowledgments: Quaid-i-Azam University, Islamabad is gratefully acknowledged for supporting this work.

Conflicts of Interest: The authors declare no conflict of interest.

References

1. Aldalbahi, A.; Mkawi, E.; Ibrahim, K.; Farrukh, M. Effect of sulfurization time on the properties of copper zinc tin sulfide thin films grown by electrochemical deposition. *Sci. Rep.* **2016**, *6*, 32431. [[CrossRef](#)] [[PubMed](#)]
2. Bartholomew, C.H. Mechanisms of catalyst deactivation. *Appl. Catal. A* **2001**, *212*, 17–60. [[CrossRef](#)]
3. Wijesinghe, M.; Perrin, K.; Ranchord, A.; Simmonds, M.; Weatherall, M.; Beasley, R. Routine use of oxygen in the treatment of myocardial infarction: Systematic review. *Heart* **2009**, *95*, 198–202. [[CrossRef](#)]

4. Kibsgaard, J.; Chen, Z.; Reinecke, B.N.; Jaramillo, T.F. Engineering the surface structure of MoS₂ to preferentially expose active edge sites for electrocatalysis. *Nat. Mater.* **2012**, *11*, 963–969. [[CrossRef](#)]
5. Li, Y.; Wang, H.; Xie, L.; Liang, Y.; Hong, G.; Dai, H. MoS₂ nanoparticles grown on graphene: An advanced catalyst for the hydrogen evolution reaction. *J. Am. Chem. Soc.* **2011**, *133*, 7296–7299. [[CrossRef](#)] [[PubMed](#)]
6. Merki, D.; Hu, X. Recent developments of molybdenum and tungsten sulfides as hydrogen evolution catalysts. *Energy Environ. Sci.* **2011**, *4*, 3878–3888. [[CrossRef](#)]
7. Vrubel, H.; Merki, D.; Hu, X. Hydrogen evolution catalyzed by MoS₃ and MoS₂ particles. *Energy Environ. Sci.* **2012**, *5*, 6136–6144. [[CrossRef](#)]
8. Hunter, B.M.; Gray, H.B.; Muller, A.M. Earth-abundant heterogeneous water oxidation catalysts. *Chem. Rev.* **2016**, *116*, 14120–14136. [[CrossRef](#)]
9. Anandhi, R.; Ravichandran, K.; Mohan, R. Conductivity enhancement of ZnO: F thin films by the deposition of SnO₂: F over layers for optoelectronic applications. *Mater. Sci. Eng. B* **2013**, *178*, 65–70. [[CrossRef](#)]
10. Carvalhal, R.F.; Sanches Freire, R.; Kubota, L.T. Polycrystalline Gold Electrodes: A Comparative Study of Pretreatment Procedures Used for Cleaning and Thiol Self-Assembly Monolayer Formation. *Electroanal. Int. J. Devoted Fundam. Pract. Asp. Electroanal.* **2005**, *17*, 1251–1259. [[CrossRef](#)]
11. Ballesteros, J.; Gomez-Solis, C.; Torres-Martinez, L.; Juárez-Ramírez, I. Electrodeposition of Cu-Zn Intermetallic Compounds for its application as Electrocatalyst in the Hydrogen Evolution Reaction. *Int. J. Electrochem. Sci.* **2015**, *10*, 2892–2903.
12. Akbar, M.; Shah, A.; Iftikhar, F.J.; Ali, G.; Han, H.; Rahman, G. In-situ formation of an efficient trimetallic (Cu-Zn-Ag) electrocatalyst for water oxidation. *Int. J. Energy Res.* **2021**, *45*, 2931–2944. [[CrossRef](#)]
13. Liu, X.; Cui, S.; Qian, M.; Sun, Z.; Du, P. In situ generated highly active copper oxide catalysts for the oxygen evolution reaction at low overpotential in alkaline solutions. *Chem. Commun.* **2016**, *52*, 5546–5549. [[CrossRef](#)] [[PubMed](#)]
14. Xiong, S.; Li, P.; Jin, Z.; Gao, T.; Wang, Y.; Guo, Y.; Xiao, D. Enhanced catalytic performance of ZnO-CoO_x electrode generated from electrochemical corrosion of Co-Zn alloy for oxygen evolution reaction. *Electrochim. Acta* **2016**, *222*, 999–1006. [[CrossRef](#)]
15. Kuang, M.; Wang, Q.; Ge, H.; Han, P.; Gu, Z.; Al-Enizi, A.M.; Zheng, G. CuCoO_x/FeOOH Core-shell nanowires as an efficient bifunctional oxygen evolution and reduction catalyst. *ACS Energy Lett.* **2017**, *2*, 2498–2505. [[CrossRef](#)]
16. Ping, J.; Wang, Y.; Lu, Q.; Chen, B.; Chen, J.; Huang, Y.; Ma, Q.; Tan, C.; Yang, J.; Cao, X. Self-assembly of single-layer CoAl-layered double hydroxide nanosheets on 3D graphene network used as highly efficient electrocatalyst for oxygen evolution reaction. *Adv. Mater.* **2016**, *28*, 7640–7645. [[CrossRef](#)] [[PubMed](#)]
17. Duan, J.; Chen, S.; Vasileff, A.; Qiao, S.Z. Anion and cation modulation in metal compounds for bifunctional overall water splitting. *ACS Nano* **2016**, *10*, 8738–8745. [[CrossRef](#)] [[PubMed](#)]
18. Ishaque, M.; Shah, A.; Iftikhar, F.J.; Akbar, M. Development of transition metal based electrolyzer for efficient oxygen evolution reaction. *J. Renew. Sustain. Energy* **2020**, *12*, 024102. [[CrossRef](#)]
19. Bahadur, A.; Hussain, W.; Iqbal, S.; Ullah, F.; Shoaib, M.; Liu, G.; Feng, K. A morphology controlled surface sulfurized CoMn₂O₄ microspike electrocatalyst for water splitting with excellent OER rate for binder-free electrocatalytic oxygen evolution. *J. Mater. Chem. A* **2021**, *9*, 12255–12264. [[CrossRef](#)]
20. Khalate, S.A.; Kadam, S.A.; Ma, Y.-R.; Kulkarni, S.B.; Parale, V.G.; Patil, U.M. Binder free cobalt iron phosphate thin films as efficient electrocatalysts for overall water splitting. *J. Colloid Interface Sci.* **2022**, *613*, 720–732. [[CrossRef](#)]
21. Geiger, S.; Kasian, O.; Mingers, A.M.; Mayrhofer, K.J.; Cherevko, S. Stability limits of tin-based electrocatalyst supports. *Sci. Rep.* **2017**, *7*, 4595. [[CrossRef](#)] [[PubMed](#)]
22. De Boer, F.; Van Santen, J.H.E.; Verwey, J.W. The electrostatic contribution to the lattice energy of some ordered spinels. *J. Chem. Phys.* **1950**, *18*, 1032–1034. [[CrossRef](#)]
23. Barakat, M.; Henaish, M.; Olofa, S.; Tawfik, A. Sintering behaviour of the spinel ferrite system Ni_{0.65}Zn_{0.35}Fe_{2-x}Cu_xO₄. *J. Therm. Anal. Calorim.* **1991**, *37*, 241–248. [[CrossRef](#)]
24. Dehnicke, K. Darstellung und Eigenschaften von SnF₂Cl₂, SnF₂(ONO₂)₂ und SnOF₂. *Chem. Ber.* **1965**, *98*, 280–289. [[CrossRef](#)]
25. Denes, G.; Pannetier, J.; Lucas, J.; Le Marouille, J. About SnF₂ stannous fluoride. I. Crystallochemistry of α-SnF₂. *J. Solid State Chem.* **1979**, *30*, 335–343. [[CrossRef](#)]
26. Hanawalt, J.; Rinn, H.; Frevel, L. Chemical analysis by X-ray diffraction. *Ind. Eng. Chem. Anal. Ed.* **1938**, *10*, 457–512. [[CrossRef](#)]
27. Pak, M.; Moshaii, A.; Siampour, H.; Abbasian, S.; Nikkhah, M. Cobalt-copper bimetallic nanostructures prepared by glancing angle deposition for non-enzymatic voltammetric determination of glucose. *Microchim. Acta* **2020**, *187*, 276. [[CrossRef](#)]
28. Esmaeeli, A.; Ghaffarinejad, A.; Zahedi, A.; Vahidi, O. Copper oxide-polyaniline nanofiber modified fluorine doped tin oxide (FTO) electrode as non-enzymatic glucose sensor. *Sens. Actuators B Chem.* **2018**, *266*, 294–301. [[CrossRef](#)]
29. Fondell, M.; Johansson, F.; Gorgoi, M.; von Feandt, L.; Boman, M.; Lindblad, A. Phase control of iron oxides grown in nano-scale structures on FTO and Si (100): Hematite, maghemite and magnetite. *Vacuum* **2015**, *117*, 85–90. [[CrossRef](#)]
30. Nickel, E. The new mineral cuprospinel (CuFe₂O₄) and other spinels from an oxidized ore dump at Baie Verte, Newfoundland. *Canad. Mineral.* **1973**, *11*, 1003–1007.
31. Dana, J.D.; Dana, E.S.; Palache, C.; Frondel, C. *System of Mineralogy: Silica Minerals*; John Wiley & Sons: New York, NY, USA, 1962; Volume 3.
32. Voncken, J.; Verkroost, T.W. Powder diffraction of cubic α-brass. *Powder Diffr.* **1997**, *12*, 228–229. [[CrossRef](#)]

33. Metsger, R.; Willman, A.; Van Ness, C. Field Guide to the Friedensville Mine of the New Jersey Zinc Company. In *Conjunction with the Northeast Section Meeting of the Geological Society of America at Allentown, Pennsylvania, March*; New Jersey Zinc Co.: Sussex, NJ, USA, 1973.
34. Kopeli, N.I.S. Electrodeposition and Characterization Of Cu-Zn Alloy Films Obtained from a Sulfate Bath. *Mater. Tehmol.* **2014**, *48*, 221–226.
35. Liu, X.; Cui, S.; Sun, Z.; Ren, Y.; Zhang, X.; Du, P. Self-supported copper oxide electrocatalyst for water oxidation at low overpotential and confirmation of its robustness by Cu K-edge X-ray absorption spectroscopy. *J. Phys. Chem. C* **2016**, *120*, 831–840. [[CrossRef](#)]
36. Song, Y.; Ichimura, M. H₂O₂ treatment of electrochemically deposited Cu₂O thin films for enhancing optical absorption. *Int. J. Photoenergy* **2013**, *2013*, 738063. [[CrossRef](#)]
37. Blanco, M.; Barragan, J.; Barelli, N.; Noce, R.; Fugivara, C.S.; Fernández, J.; Benedetti, A.V. On the electrochemical behavior of Cu–16% Zn–6.5% Al alloy containing the β'-phase (martensite) in borate buffer. *Electrochim. Acta* **2013**, *107*, 238–247. [[CrossRef](#)]
38. Hacıbrahimoglu, M.Y.; Bedir, M.; Yavuz, A. Structural and Corrosion Study of Uncoated and Zn-Cu Coated Magnesium-Based Alloy. *Metals* **2016**, *6*, 322. [[CrossRef](#)]
39. Haque, F.; Rahman, M.; Ahmed, E.; Bakshi, P.; Shaikh, A. A Cyclic Voltammetric Study of the Redox Reaction of Cu (II) in Presence of Ascorbic Acid in Different pH Media. *Dhaka Univ. J. Sci.* **2013**, *61*, 161–166. [[CrossRef](#)]
40. Khelladi, M.; Mentar, L.; Boubatra, M.; Azizi, A. Study of nucleation and growth process of electrochemically synthesized ZnO nanostructures. *Mater. Lett.* **2012**, *67*, 331–333. [[CrossRef](#)]
41. Li, H.; Xu, C.; Han, C.; Chen, Y.; Wei, C.; Li, B.; Kang, F. Enhancement on cycle performance of Zn anodes by activated carbon modification for neutral rechargeable zinc ion batteries. *J. Electrochem. Soc.* **2015**, *162*, A1439–A1444. [[CrossRef](#)]
42. Mentar, L. A study of the electrodeposition of Co–Cu alloys thin films on FTO substrate. *Ionics* **2012**, *18*, 223–229. [[CrossRef](#)]
43. Suen, N.-T.; Hung, S.-F.; Quan, Q.; Zhang, N.; Xu, Y.-J.; Chen, H.M. Electrocatalysis for the oxygen evolution reaction: Recent development and future perspectives. *Chem. Soc. Rev.* **2017**, *46*, 337–365. [[CrossRef](#)]
44. Wei, L.; Karahan, H.E.; Zhai, S.; Liu, H.; Chen, X.; Zhou, Z.; Lei, Y.; Liu, Z.; Chen, Y. Amorphous bimetallic oxide–graphene hybrids as bifunctional oxygen electrocatalysts for rechargeable Zn–air batteries. *Adv. Mater.* **2017**, *29*, 1701410. [[CrossRef](#)] [[PubMed](#)]
45. Zhao, Z.; Gu, F.; Li, Y.; Sun, W.; Ye, S.; Rao, H.; Liu, Z.; Bian, Z.; Huang, C. Mixed-organic-cation tin iodide for lead-free perovskite solar cells with an efficiency of 8.12%. *Adv. Sci.* **2017**, *4*, 1700204. [[CrossRef](#)] [[PubMed](#)]
46. Tang, D.; Han, Y.; Ji, W.; Qiao, S.; Zhou, X.; Liu, R.; Han, X.; Huang, H.; Liu, Y.; Kang, Z. A high-performance reduced graphene oxide/ZnCo layered double hydroxide electrocatalyst for efficient water oxidation. *Dalton Trans.* **2014**, *43*, 15119–15125. [[CrossRef](#)] [[PubMed](#)]
47. Lu, Z.; Qian, L.; Tian, Y.; Li, Y.; Sun, X.; Duan, X. Ternary NiFeMn layered double hydroxides as highly-efficient oxygen evolution catalysts. *Chem. Commun.* **2016**, *52*, 908–911. [[CrossRef](#)] [[PubMed](#)]
48. Dong, C.; Kou, T.; Gao, H.; Peng, Z.; Zhang, Z. Eutectic-derived mesoporous Ni-Fe-O nanowire network catalyzing oxygen evolution and overall water splitting. *Adv. Energy Mater.* **2018**, *8*, 1701347. [[CrossRef](#)]
49. Lin, X.; Li, X.; Li, F.; Fang, Y.; Tian, M.; An, X.; Fu, Y.; Jin, J.; Ma, J. Precious-metal-free Co–Fe–O_x coupled nitrogen-enriched porous carbon nanosheets derived from Schiff-base porous polymers as superior electrocatalysts for the oxygen evolution reaction. *J. Mater. Chem. A* **2016**, *4*, 6505–6512. [[CrossRef](#)]
50. Li, X.; Ye, N.; Liu, H.; Li, C.; Huang, Y.; Zhu, X.; Feng, H.; Lin, J.; Huang, L.; Wu, J.; et al. Bifunctional iron doped CuS catalysts towards highly efficient overall water electrolysis in the alkaline electrolyte. *Int. J. Hydrogen Energy* **2022**, *47*, 16719–16728. [[CrossRef](#)]
51. Wang, Z.; Qian, G.; Yu, T.; Chen, J.; Shen, F.; Luo, L.; Zou, Y.; Yin, S. Carbon encapsulated FeWO₄-Ni₃S₂ nanosheets as a highly active catalyst for overall water splitting at large current density. *Chem. Eng. J.* **2022**, *434*, 134669. [[CrossRef](#)]
52. Fatemeh Yaghoubidoust, F.; Wicaksono, D.H.B.; Chandren, S.; Nur, H. Effect of graphene oxide on the structural and electrochemical behavior of polypyrrole deposited on cotton fabric. *J. Molec. Struct.* **2014**, *1075*, 486–493. [[CrossRef](#)]
53. Nimal, R.; Yahya, R.; Shah, A.; Khan, M.A.; Zia, M.A.; Shah, I. Development of Electrolyzer Using NiCo(OH)₂ Layered Double Hydroxide Catalyst for Efficient Water Oxidation Reaction. *Nanomaterials* **2022**, *12*, 1819. [[CrossRef](#)] [[PubMed](#)]